

January 2008

Stick-slip motions in the friction force microscope: Effects of tip compliance

William G. Conley

Purdue University, wconley@purdue.edu

Charles M. Krousgrill

Purdue University, krousgrill@purdue.edu

Arvind Raman

Birck Nanotechnology Center, Purdue University, raman@purdue.edu

Follow this and additional works at: <http://docs.lib.purdue.edu/nanopub>

Conley, William G.; Krousgrill, Charles M.; and Raman, Arvind, "Stick-slip motions in the friction force microscope: Effects of tip compliance" (2008). *Birck and NCN Publications*. Paper 205.

<http://docs.lib.purdue.edu/nanopub/205>

This document has been made available through Purdue e-Pubs, a service of the Purdue University Libraries. Please contact epubs@purdue.edu for additional information.

Stick-Slip Motions in the Friction Force Microscope: Effects of Tip Compliance

William G. Conley · Charles M. Krousgrill · Arvind Raman

Received: 10 May 2007 / Accepted: 16 October 2007 / Published online: 3 November 2007
© Springer Science+Business Media, LLC 2007

Abstract When a microcantilever with a nanoscale tip is scanned laterally over a surface to measure the nanoscale frictional forces, the onset of stick-slip tip motions is an extremely important phenomenon that signals the onset of lateral friction forces. In this article, we investigate theoretically the influence of tip and microcantilever compliance on this phenomenon. We show that static considerations alone cannot predict uniquely the onset of single or multiple atom slip events. Instead, the nonlinear dynamics of the tip during a slip event need to be carefully investigated to determine if the tip evolves to a single or multiple atom stick-slip motions. The results suggest that the relative compliances of the tip and microcantilever can be engineered to induce single or multiple atom stick-slip events and thus control lateral friction forces at the nanoscale.

Keywords AFM · Dynamic modeling · Stick-slip · Nanotribology · Friction mechanisms

1 Introduction

Friction force microscopy (FFM) [1] is an experimental tool that provides insight into the atomic origin of friction by measuring frictional forces at the nanoscale. In FFM, a microcantilever with a nanoscale tip is brought into the repulsive regime of tip-sample interaction. The microcantilever is then scanned laterally over a sample, while the friction forces on the tip are measured indirectly by monitoring the torsional deflection of the cantilever, as shown in Fig. 1a. FFM has been used to measure: (a) atomic-scale stick-slip phenomena over single [2] or multiple atoms [3], (b) the dependence of nanoscale friction on normal load leading to the demonstration of a new regime of superlubricity [4], and (c) the reduction in nanoscale frictional forces due to imposed high-frequency vibrations [5–7]. In order to develop a theoretical basis for these and other observed experimental results in FFM, reduced order models of the elastic cantilever and tip sliding over atomic lattices are needed [8–10]. The most common model used for this purpose is Tomlinson’s model [11].

Tomlinson’s model assumes that the nanoscale tip is rigid, and therefore, ignores the effects of tip compliance in FFM. Tip compliance (Fig. 1b) is likely to play an important role in FFM, especially when the lateral surface force gradients are large such as for surfaces with high adhesion or for tips under larger normal loads, or when a high aspect ratio tip is used. While tip compliance is an issue in conventional FFM (Fig. 1b), it bears even greater importance for emerging carbon nanotube (CNT-FFM) probes [12], as shown in Fig. 1a. Some other techniques for examining tip compliance exist. For instance, molecular dynamics (MD) calculations can be used to study the effect of tip compliance [13]. However, extracting simple relationships from MD results can be quite challenging.

W. G. Conley
School of Mechanical Engineering and Birck Nanotechnology
Center, Purdue University, 1205 West State Street,
West Lafayette, IN 47907, USA

C. M. Krousgrill
School of Mechanical Engineering, Purdue University,
585 Purdue Mall, West Lafayette, IN 47907, USA

A. Raman (✉)
School of Mechanical Engineering and Birck Nanotechnology
Center, Purdue University, 585 Purdue Mall, West Lafayette, IN
47907, USA
e-mail: raman@ecn.purdue.edu

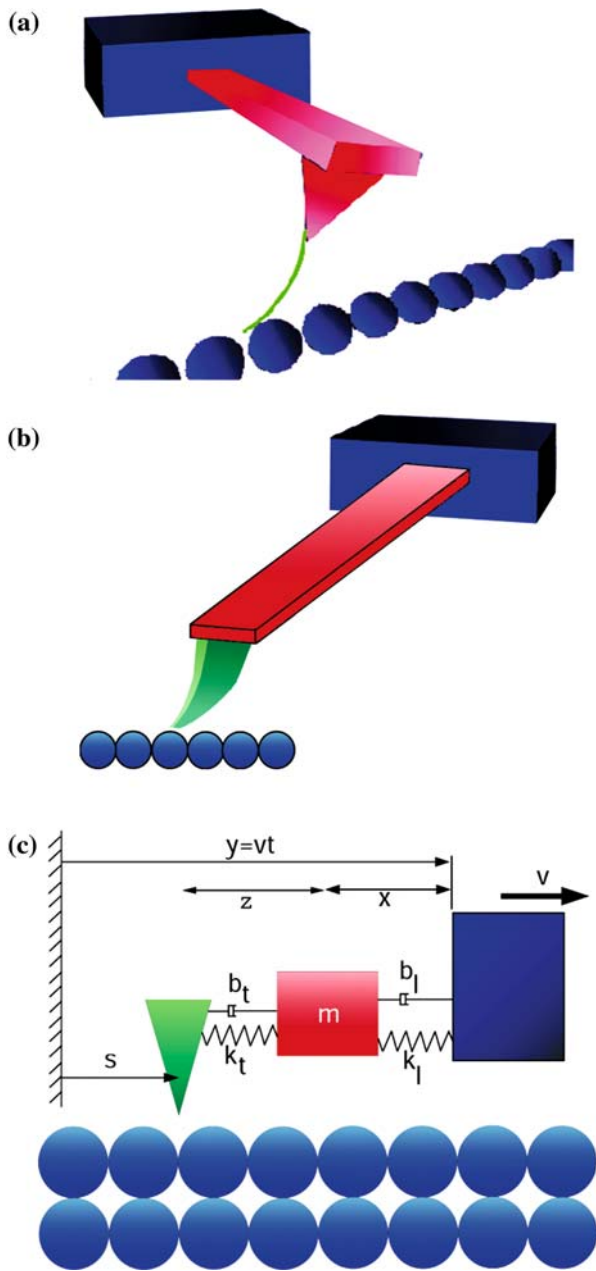


Fig. 1 Schematics showing different mechanisms tip compliance in friction force microscopy: (a) Flexure of carbon nanotube tips and (b) tip deformation of conventional tips due to high aspect ratio or due to high lateral surface force gradients. (c) A reduced order model applicable to both cases

Moreover, in Luan and Robbins [13], a constant force is applied to the base of the slider. Our interest lies in simple models for predicting stick-slip dynamics when the slider base is moved at a constant velocity which is more relevant to FFM. Therefore, simple, reduced order models, which capture the essential physics including the effects of tip compliance, are quite useful. Johnson and Woodhouse [14] extended Tomlinson's model to include a finite compliance

of the tip, representing it in the reduced order model as a compliant spring. This model [14] neglects the small but finite mass of the compliant tip under the assumption that the natural frequency of the nanoscale tip is far greater than that of the cantilever, thus requiring the tip to respond infinitely fast as it slips to the next atom in the lattice.

The present work seeks to improve upon previous models by developing a physically motivated model of a FFM microcantilever coupled to the lattice through a compliant tip. Additionally, the present work: (1) provides correct analytical values of the effective tip-cantilever compliance at which a specific number of atoms may be bypassed during a stick-slip event, (2) determines the boundary in parameter space between single and multiple atom stick-slip motions, (3) studies the effects of microcantilever and tip damping on multiple atom stick-slip motions, and (4) describes the implications of tip compliance on the lateral forces measured in experimental FFM.

2 Model

Figure 1c shows a reduced order model which describes an FFM microcantilever with a compliant tip in contact with a sample lattice. The lattice being scanned is assumed to be rigid and the interaction potential for the surface lateral forces is assumed to be spatially harmonic, just as in Tomlinson's model [15]. The equations of motion of the microcantilever and tip are:

$$m \frac{d^2 x}{dt^2} + b_l \frac{dx}{dt} + k_l x = T^{\star} \sin \frac{2\pi s}{\lambda} \quad (1)$$

$$b_t \left(\frac{ds}{dt} - v + \frac{dx}{dt} \right) + k_t (s - y + x) = -T^{\star} \sin \frac{2\pi s}{\lambda}.$$

The deflection of the end of the microcantilever relative to the base is x and the deflection of the tip relative to the end of the microcantilever is z . The base motion of the microcantilever, y , is assumed to be moving at a constant velocity v , thus $y = vt$. The absolute position of the tip is s . The different coordinates are algebraically related by $y = s + x + z$. The reduced order model has effective mass m , stiffness k_l , and damping b_l , respectively, representing the suspended mass, stiffness, and damping of the torsional motion of microcantilever. Additionally, the tip possesses stiffness k_t and damping coefficient b_t . For stiff elastic samples, k_t captures the effective stiffness of both the tip and sample [16, 17]. However, if the sample is very compliant, the above model is not sufficient and additional equations describing the motion of the surface atoms need to be considered.

This model builds upon the work of Johnson and Woodhouse [14] by including a realistic finite time scale associated with the slipping motion of the tip. Additionally, as $k_t \rightarrow \infty$, the model reduces to the well-studied

Tomlinson’s model [8]. The force required to slide the base of the microcantilever at constant velocity is $f_l = k_l x + b_l \dot{x}$. However, the lateral force measured in FFM experimentally is proportional only to the elastic (torsional) deflection of the microcantilever, $f_{meas} = k_l x$.

To aid in generalizing the results of this model, the following substitutions are used to non-dimensionalize Eq. 1:

$$\begin{aligned} S &= s/\lambda, & Y &= y/\lambda, & X &= x/\lambda, \\ \omega_l &= \sqrt{\frac{k_l}{m}}, & C_t &= T^{*}/\lambda k_t, & C_l &= T^{*}/\lambda k_l, \\ \delta_l &= b_l \omega_l / 2k_l, & \delta_t &= b_t \omega_t / 2k_t, & q &= \omega_l t. \end{aligned} \tag{2}$$

The non-dimensional equations of motion then reduce to:

$$\begin{aligned} \frac{d^2 X}{dq^2} + 2\delta_l \frac{dX}{dq} + X &= C_l \sin(2\pi S) \\ 2\delta_t \left(\frac{dY}{dq} - \frac{dS}{dq} - \frac{dX}{dq} \right) + Y - S - X &= C_t \sin(2\pi S). \end{aligned} \tag{3}$$

C_l can be regarded as the ratio of the microcantilever compliance to the lateral surface compliance (inverse of lateral force gradient), while C_t is the ratio of tip compliance to lateral surface compliance. The damping ratio of the microcantilever is δ_l , while the tip damping ratio is δ_t . Critical damping of a free microcantilever corresponds to $\delta_l = 1$. In terms of these non-dimensional quantities the force required to slide the base at a constant velocity becomes $F_t = \frac{X}{C_l} + \frac{2\delta_l}{C_l} \frac{dX}{dq}$ and the lateral force measured in a FFM experiment becomes $F_{meas} = \frac{X}{C_l}$, since the experimental measurement relies on measuring the deflection of the microcantilever.

The non-dimensional quantities in Eq. 3 depend on both the material and geometric properties of the microcantilever, tip, and sample. For example, the microcantilever and tip compliances (C_l and C_t , respectively) depend on their elastic moduli and geometry; longer microcantilevers and tips are more compliant. The surface lateral compliance depends on the applied normal load and lattice spacing; larger applied normal loads decrease the surface lateral compliance, while smaller interatomic distance of the lattice increases the surface lateral compliance. The damping in the microcantilever, δ_l , is due to both air damping and internal material damping; damping of the tip oscillations, δ_t , is likely to arise from the generation of phonons in the lattice as slipping occurs between the tip and lattice.

This model improves upon that of Johnson and Woodhouse [14] by including a physically realistic finite timescale of the tip motion because infinitely fast tip response times can lead to non-physical simulation results. Our objective is to use the compliant tip model (Eq. 3) to investigate the mechanisms of multiple atom stick-slip events in FFM. In what follows, the equilibria and dynamics of Eq. 3 are investigated systematically. First, a quasi-static model is considered in Sect. 3 when the sliding velocity is infinitesimally slow. Next, an analysis of the

dynamic effects on multiple atom stick-slip motions is performed as the microcantilever and tip compliances are systematically varied in Sect. 4. Finally, the implications of multiple atom stick-slip on the average frictional force measured in FFM are described in Sect. 5 and the conclusions are presented in Sect. 6.

3 Quasi-static Analysis

In this section, we investigate the equilibria of Eq. 3 for vanishing sliding velocities (quasi-static assumption). In this approximation, all velocities and accelerations are set to zero ($V \rightarrow 0$, $\frac{dx}{dq} \rightarrow 0$, $\frac{d^2x}{dq^2} \rightarrow 0$, and $\frac{dz}{dt} \rightarrow 0$), thereby simplifying the coupled equations (3) to a single algebraic equation:

$$Y^* = S^* + C_e \sin(2\pi S^*), \tag{4}$$

where $C_e \equiv C_t + C_l$ is the *effective compliance* of the combined microcantilever and tip and (Y^*, S^*) is an equilibrium solution. In the quasi-static approximation, the non-dimensional force measured in FFM is:

$$F_{meas}^* = \frac{X^*}{C_l} = \sin(2\pi S^*). \tag{5}$$

In an experiment, the base position of the microcantilever, Y^* , is prescribed. Our interest lies in the position of the tip, S^* , from which the lateral friction force can be directly derived by Eq. 5. Once an equilibrium solution (Y^*, S^*) is found, its Liapunov stability is determined via the Lagrange–Dirichlet criterion, by examining the curvature of the potential energy:

$$\left. \frac{d^2 U}{dS^2} \right|_{Y=Y^*, S=S^*} = \left. \frac{d^2}{dS^2} \left(\frac{1}{2C_e} (Y-S)^2 - \frac{1}{2\pi} \cos(2\pi S) \right) \right|_{Y=Y^*, S=S^*}. \tag{6}$$

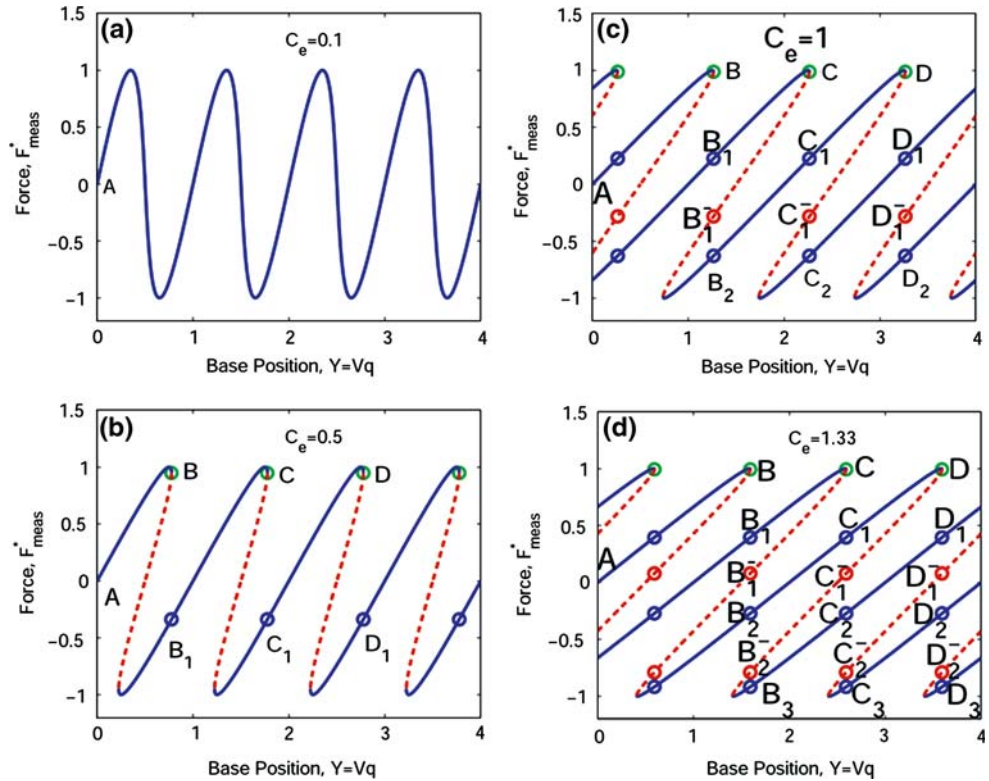
For a stable equilibrium, the curvature is positive.

Next, the qualitative dependence of the equilibrium position, S^* , as a function of the position of the base of the microcantilever, Y^* , and effective compliance, C_e , is investigated. Equilibrium solutions (Y^*, S^*) are found via Eq. 4 for continuously varying S^* and the stability of each equilibrium is determined by Eq. 6.

When $C_e = 0.1$, Fig. 2a shows the measured lateral force, F_{meas}^* , as the base position of the microcantilever is varied. The lateral force begins at the point A and varies smoothly for all Y^* .

When the effective compliance, C_e , is increased to $C_e = 0.5$ a fundamental change occurs, as shown in Fig. 2b. The figure shows the variation of the lateral force, F_{meas}^* , as the base position, Y^* , varies. The lateral force, F_{meas}^* , begins at point A and remains associated with a local equilibrium until the point B. As Y^* increases beyond B, the

Fig. 2 Plots of quasi-static lateral force, $F_{\text{meas}}^*(Y^*) = X^*/C_e = \sin(2\pi S^*)$ as a function of base position Y , for increasing effective compliances. Stable solutions are represented by solid lines, while unstable solutions are represented by dashed lines. (a) Steady sliding for $C_e = 0.1$, (b) Single atom stick-slip motion (SASSM) for $C_e = 0.5$ as the tip follows the path $A - B - B_1$, (c) For $C_e = 1$, two possibilities exist, either the tip follows a SASSM $A - B - B_1 - C - C_1$ or a double atom stick-slip motion (DASSM) $A - B - B_2 - D - D_1$, (d) For $C_e = 1.33$, multiple possibilities arise for tip motion including a SASSM ($A - B - B_1 - C - C_1 - D - D_1$), DASSM ($A - B - B_2 - D - D_2$), or triple atom stick-slip motion (TASSM) ($A - B - B_3$)



tip transitions to the equilibrium at B_1 . It is easy to observe that the only motion possible is $A - B - B_1$, and this motion repeats itself with a spatial periodicity identical to the atomic spacing. We refer to this periodic motion as a single atom stick-slip motion (SASSM).

If the effective compliance increases to $C_e = 1$, another fundamental change occurs as shown in Fig. 2c. The tip begins at point A and remains associated with the local equilibrium until the point B . However, two different local equilibria now exist beyond B . The tip may become associated with the equilibria B_1 or B_2 . Thus, two different motions are possible, the path $A - B - B_1 - C - C_1$ or $A - B - B_2$. The first path corresponds to a SASSM since the tip moves approximately one lattice spacing between B and B_1 , while the second path is a double atom stick-slip motion (DASSM) since the tip moves approximately two lattice spacings between B and B_2 .

If the effective compliance is increased even more to $C_e = 1.33$, again the number of stable equilibria increases, as shown in Fig. 2d. Beyond B , three possible stable equilibrium are possible, B_1 , B_2 , and B_3 . These result in three possible periodic stick-slip motions: (a) a SASSM follows the path $A - B - B_1 - C - C_1 - D - D_1$, while (b) a DASSM follows the path $A - B - B_2 - D - D_2$, and (c) a triple atom stick-slip motion (TASSM) follows the path $A - B - B_3$. Note that the TASSM path has a slip length of approximately three lattice spacings.

In Fig. 2, while the stable solutions $B_n, C_n,$ and D_n ($n = 1, 2, \dots$) are called nodes and the unstable solutions B_n^- ($n = 1, 2, \dots$) are called saddles, the points $B, C,$ and D are called saddle-node bifurcations according to the language of bifurcation theory [18]. A saddle-node bifurcation occurs when a stable node and an unstable saddle combine and annihilate each other. It is helpful to record here analytical expressions for the position of the saddle-node bifurcation, $(Y_{\text{SN}}^*, S_{\text{SN}}^*)$. At the saddle-node bifurcation [18]

$$\left(\frac{d[C_e \sin(2\pi S^*)]}{dY^*} \right) \Big|_{Y^*=Y_{\text{SN}}^*} = \infty. \tag{7}$$

Solving Eq. 7 simultaneously with Eq. 4 leads to the following expression for $(Y_{\text{SN}}^*, S_{\text{SN}}^*)$:

$$\begin{aligned} S_{\text{SN}}^* &= \frac{1}{2\pi} \arccos\left(-\frac{1}{2\pi C_e}\right) \\ Y_{\text{SN}}^* &= S_{\text{SN}}^* + C_e \sin(2\pi S_{\text{SN}}^*) \\ &= \frac{1}{2\pi} \arccos\left(-\frac{1}{2\pi C_e}\right) + C_e \sin\left[\arccos\left(-\frac{1}{2\pi C_e}\right)\right]. \end{aligned} \tag{8}$$

In addition to providing knowledge of the positions of the saddle-node bifurcations, the quasi-static model also helps to determine the critical values of effective compliance, $C_e^{(n)}$, which separate the possibility of $n - 1$ atoms being involved in the slip event from n atoms being

involved in the slip event. For example if $C_e < C_e^{(1)}$, then only steady sliding occurs. However, if $C_e^{(1)} < C_e < C_e^{(2)}$, then a SASSM occurs. If $C_e^{(2)} < C_e < C_e^{(3)}$, then either a SASSM or DASSM may occur; the only way to resolve which of the two possibilities actually occurs is to numerically simulate the nonlinear dynamics of Eq. 3. This issue is discussed in Sect. 4. However, the $C_e^{(n)}$ values nevertheless provide an expectation on the dynamic behavior of Eq. 3.

To determine the critical values of effective compliance, $C_e^{(n)}$, from Eq. 8, we observe from Fig. 2 that the force curves are anti-symmetric about the origin. To find the critical $C_e^{(n)}$ values, therefore, we must solve Eq. 8 together with the requirement:

$$Y^*(S_{SN}^*) = Y^*(-S_{SN}^*) + n, \quad (9)$$

where n is any positive integer. For $n = 1$, an analytical solution exists $C_e^{(1)} = 1/(2\pi)$. For $n > 1$, Eqs. 8 and 9 need to be solved numerically, for example $C_e^{(2)} = 0.733$. If $C_e < C_e^{(1)}$, then steady sliding occurs. If $C_e^{(1)} < C_e < C_e^{(2)}$, then the only possible solution is SASSM. If $C_e^{(2)} < C_e < C_e^{(3)}$, then either a SASSM or a DASSM is possible. This logic is applicable to higher number of atomic stick-slip events as well.

The quasi-static equilibrium analysis thus provides an understanding of the different co-existing stick-slip motions. The conditions presented here are different than those of Johnson and Woodhouse [14]. The maximum compression of the cantilever in Appendix B of [14] is not the proper condition for multiple atom stick-slip motions.

4 Dynamic Response

During the sudden release of the tip as it snaps to the next atom, the dynamics of Eq. 3 must be examined in order to determine how many atoms the tip slides over. The quasi-static model simply determines the number of atoms over which the tip *may* slip. However, specific damping (δ_t , δ_l) and compliance values (C_t , C_l) in both the microcantilever and tip must be individually investigated to determine how many atoms are *actually* involved in the dynamic stick-slip motion. The sliding velocity is set to be very slow $V = \frac{dY}{dt} = 10^{-6}$ for all the simulations in the present work. Additionally, initial conditions are chosen at a time just before the saddle-node bifurcation (point B), at time q_{IC} . We begin at $Y(q_{IC}) = 0.998Y_{SN}^*$ and then numerically solve for $S(q_{IC})$ using Eq. 4. Then the quasi-static relation $X(q_{IC}) = Y(q_{IC}) - S(q_{IC}) - C_t \sin(2\pi S(q_{IC}))$ is used to determine the initial microcantilever deflection. Lastly, $\dot{X}(q_{IC}) = 0$ is specified. All the simulations are performed in Matlab using ODE45 with the default integration tolerances.

In what follows, we will summarize results from numerical simulations performed over a wide range of compliance values (C_t , C_l). We vary the tip compliance C_t from 0 (a very rigid tip, and very low lateral surface force gradient) to 0.6 (very compliant tip and large lateral surface force gradient). The microcantilever compliance C_l is varied from 0 (a very rigid microcantilever and very low lateral surface gradient) to 1.6 (very compliant microcantilever and large lateral surface force gradient). The microcantilever dissipation (δ_l) is varied; both a “high” and a “low” dissipation case is considered. For comparison between the two different microcantilever dissipation cases, the tip damping (δ_t) is maintained at a constant low value. To facilitate a comparison with the previous section, the time history of the lateral force, F_{meas} , is plotted from the dynamic simulations.

4.1 Dynamic Stick-Slip Events with Highly Damped Microcantilevers

We begin by considering a highly damped (high δ_l) microcantilever. Following Johnson and Woodhouse [14], we set the microcantilever damping, $\delta_l = 0.1$. Since no experimental data has been reported on plausible values of tip damping, we will assume $\delta_t = 0.025$. While a comprehensive study of the dependence of our results on δ_t is beyond the scope of this work, the computations are qualitatively comparable for a wide range of δ_t . The results remain qualitatively similar when δ_t is varied by an order of magnitude. If δ_t is increased by several orders of magnitude, the results approach the well-studied [15] single degree of freedom of Tomlinson’s model.

While the effective compliance, C_e , determines entirely the response in the quasi-static model, the numerical integrations of the *dynamic* Eq. 3 indicate otherwise. For example in Fig. 3a, the choice $(C_t, C_l) = (0.21, 0.79)$ yields $C_e = 1$ and results in a SASSM when Eq. 3 is numerically integrated. However, while maintaining $C_e = 1$ if the tip and the sample compliance are varied to $(C_t, C_l) = (0.20, 0.80)$, then a DASSM occurs, as shown in Fig. 3b. Note that in both Fig. 3a and 3b, the measured lateral force, F_{meas} , is plotted as a function of scaled time. It is instructive to plot in 2-D phase space the cantilever oscillations over one period of stick-slip. The phase space diagrams for $C_e = 1$, $(C_t, C_l) = (0.21, 0.79)$, and $(C_t, C_l) = (0.20, 0.80)$ in Fig. 3c also show the saddle-node bifurcation B and stable equilibria B_1 and B_2 corresponding to the points labeled in Fig. 2c. The positions of the saddle-node bifurcation B and the nodes B_1 and B_2 , and saddles B_1^- change imperceptibly when $(C_t, C_l) = (0.21, 0.79)$ changes to $(C_t, C_l) = (0.20, 0.80)$. However, following a saddle-node bifurcation the tip in the former

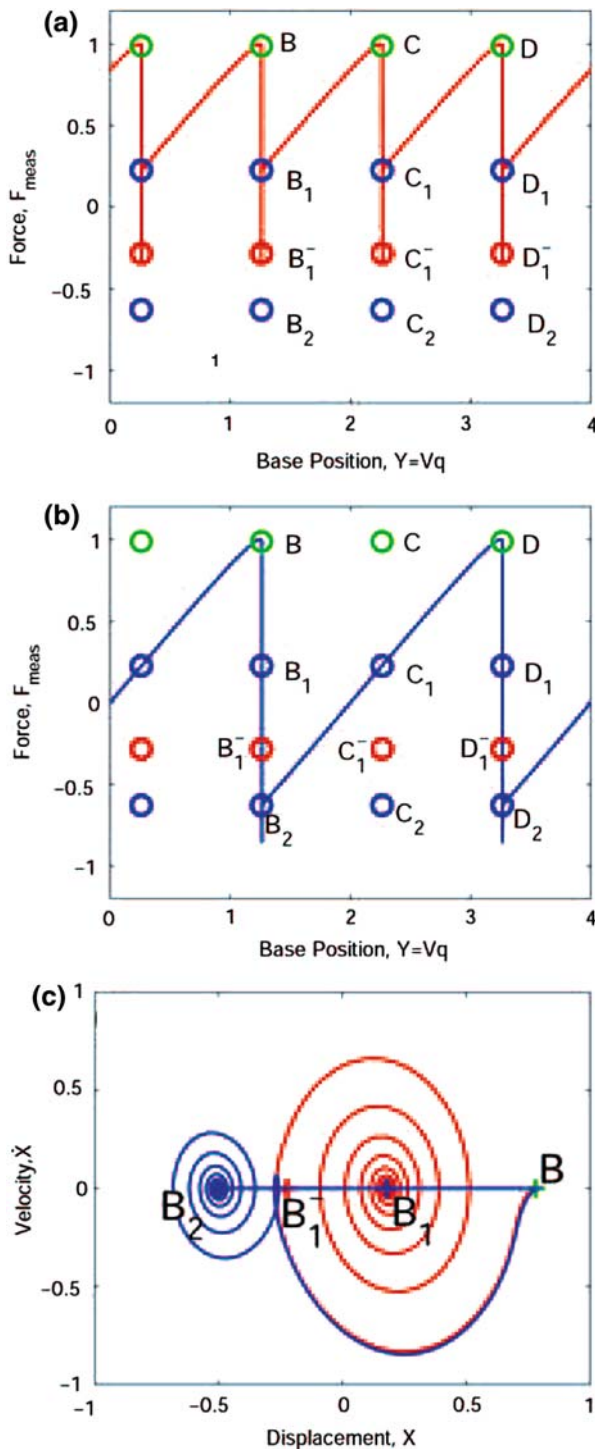


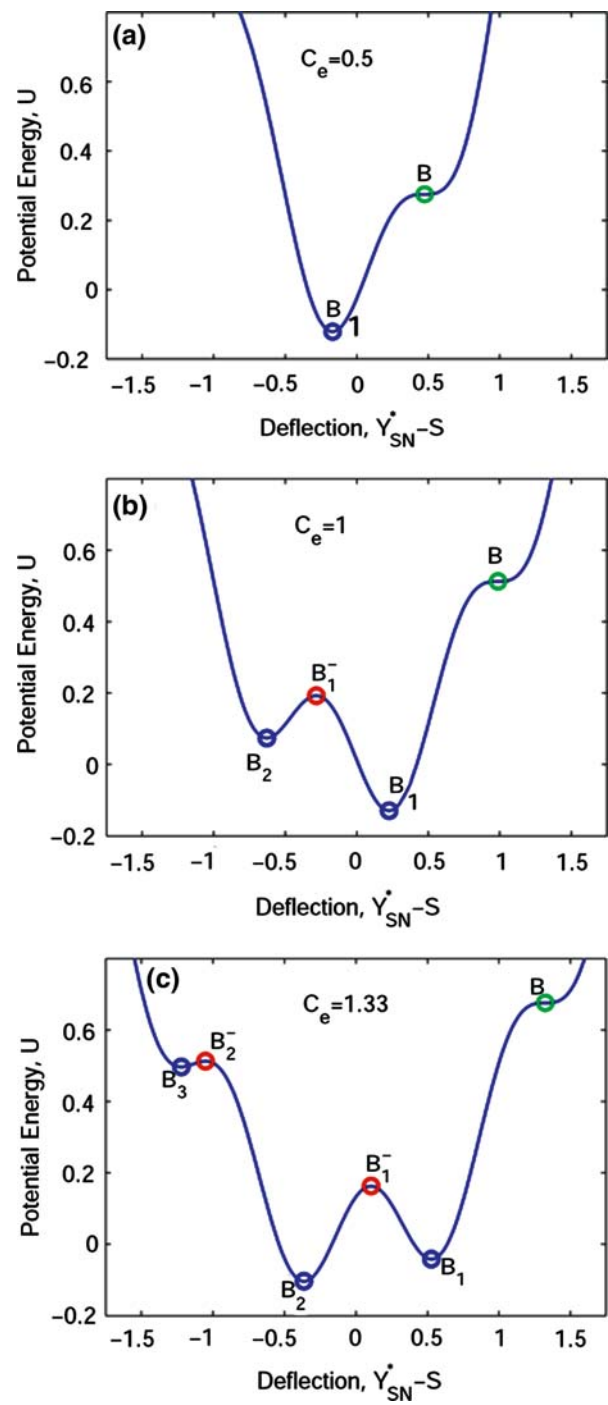
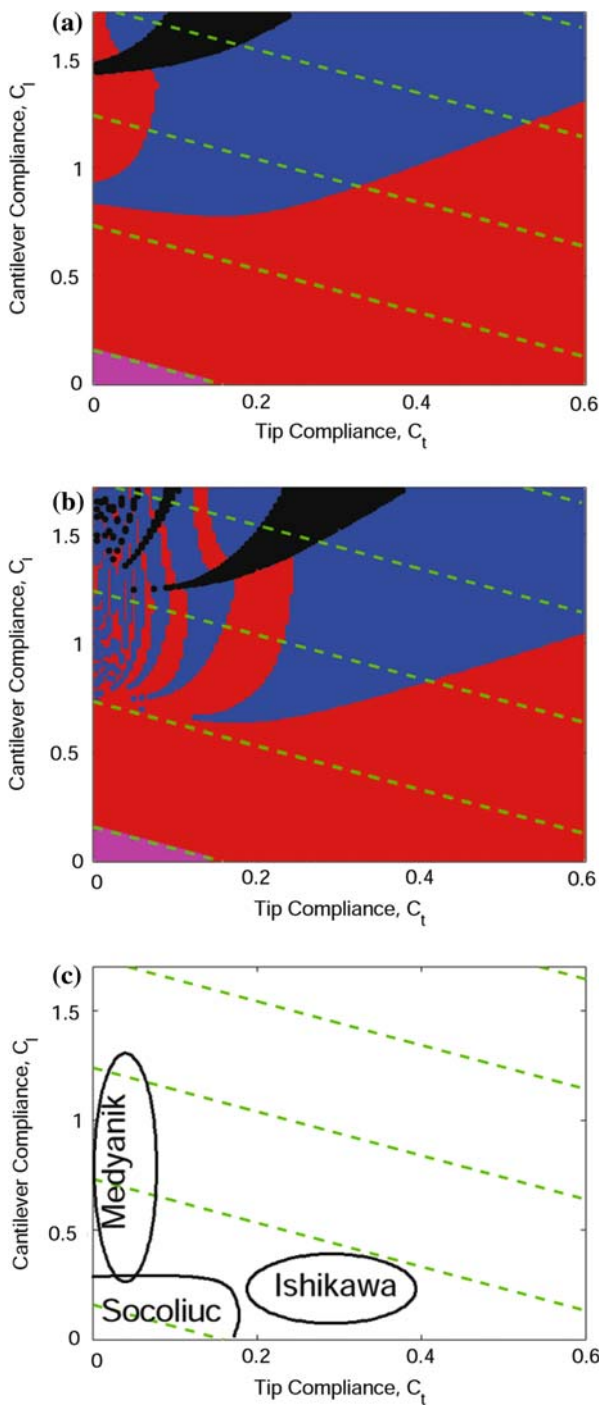
Fig. 3 (a) The measured lateral force F_{meas} as a function of dimensionless time, when tip dynamics Eq. 3 are numerically integrated for $C_t = 0.21$, and $C_l = 0.79$, shows that the tip motion settles into a periodic SASSM. (b) If $C_t = 0.2$ and $C_l = 0.8$, the tip settles into a periodic DASSM (Note that in (a) and (b) the effective compliance $C_e = 1$ is identical), and (c) 2-D phase space projection of the results in (a) and (b). The labels B , B_1 , B_1^- , and B_2 correspond to those in Fig. 2

Fig. 4 Results of numerical integration showing regions of steady sliding (magenta), SASSM (red), DASSM (blue), and TASSM (black) for (a) $\delta_t = 0.1$ and $\delta_r = 0.025$ and (b) $\delta_t = 0.001$ and $\delta_r = 0.025$. The dashed lines are lines of constant C_e separating increasing number of atoms involved in the stick-slip motion. The dashed lines predict possible transitions from one type of stick-slip motion to another and arise from static considerations alone. However, the colored/shaded regions are the tip motions that arise once the dynamic equations of motion (3) are carefully integrated. The differences arise fundamentally due to nonlinear dynamic transients following a stick-slip event that predisposes the tip to the attractive basin of a specific equilibrium. The increasing complexity of (b) when compared to (a) is due to the lower level of microcantilever damping. The tip and microcantilever may circle the saddles multiple times before becoming associated with an individual atom. (c) The regions demarcated represent the experimental work of Medyanik et al. [3], Socoliuc et al. [4], and Ishikawa et al. [12]. Substantial regions of parameter space remain to be explored to better understand multiple atom stick-slip motions

case decays into B_1 and the other into B_2 in the latter case. This indicates that, while the effective compliance, $C_e \equiv C_t + C_l$, determines the equilibria and saddle-node bifurcations, the specific values of C_t and C_l determine the domains of attraction for the SASSMs and DASSMs.

The above simulations are performed over a wide range of compliance values, (C_t, C_l) , and Fig. 4a shows the regions in (C_t, C_l) space that lead to steady sliding, SASSM, DASSM, and TASSM. The dashed lines correspond to $C_e^{(n)}$ values from Sect. 3 for $n \leq 4$. Note, however, that the regions for $C_e < C_e^{(2)}$ do not require numerical simulation and are plotted using the analytical criteria described in Sect. 3. Several key results are observed from this figure and described systematically:

- Continuous, smooth boundaries in (C_t, C_l) space separate SASSM, DASSM, and TASSM.
- Even though C_e may be large enough for a DASSM to occur based on the quasi-static model, a much larger C_e value is required for DASSM to actually occur when the dynamics are taken into account. This can be understood by considering the potential energy wells for different values of C_e . The wells are calculated from the potential energy Eq. 6 and plotted in Fig. 5 for varying C_e when $Y = Y_{SN}^*(C_e)$, which corresponds to the base position at the moment of slip. The tip begins at the start of stick-slip motion at the saddle-node bifurcation A with energy $U(S_{SN}^*, Y_{SN}^*)$. For small C_e values (Fig. 5a), only one stable equilibrium (B_1) is present, and the tip converges toward this stable equilibrium due to damping. If $C_e^{(2)} < C_e < C_e^{(3)}$, as shown in Fig. 5b, the tip transitions to either of two stable equilibria (B_1 or B_2) depending on the damping values. As C_e continues to increase, as shown in Fig. 5c, then the tip transitions to one of three stable



equilibria (B_1 , B_2 , or B_3). Clearly, as C_e increases, so does the likelihood of occurrence of either a DASSM or TASSM. While a TASSM is possible according to the quasi-static model for $C_e = 1.33$ in Fig. 5c, the probability of this motion is very small since the potential energy at the saddle, B_2^- , is very close to the potential energy of the saddle node bifurcation, A . In the presence of damping, the tip may not cross the unstable equilibrium B_2^- .

Fig. 5 Potential energy landscape when the tip is just about to undergo a stick-slip motion and is located at a saddle point. The potential energies are plotted as a function of combined cantilever-tip deflection, $Y_{SN}^* - S$. The labeled points, B , B_1 , B_1^- , B_2 , B_2^- , and B_3 correspond to those in Fig. 2. The potential energies are plotted for different effective compliance values (a) $C_e = 0.5$, (b) $C_e = 1$, and (c) $C_e = 1.33$

- The key differences between our results and those of Johnson and Woodhouse [14] are that we observe multiple boundaries in (C_t, C_l) space separating

SASSM and DASSM in Fig. 4a. Moreover, unlike Johnson and Woodhouse, we also observe TASSM. These differences are detected by performing numerical integrations over a larger region of parameter space (C_t, C_l).

4.2 Dynamic Stick-Slip Events in Slightly Damped Microcantilevers

Now that a thorough understanding of single and multiple atom stick-slip of a high dissipation microcantilever has been developed, it is interesting to consider a lower dissipation microcantilever. Sharos et al. [19] measured the quality factors of torsional and lateral modes of microcantilevers in air to be 700–800. This is a much higher quality factor than the previous case considered and corresponds to microcantilever damping of $\delta_l = 0.000625 - 0.000714$. To evaluate the effect of low damping, we select $\delta_l = 0.001$; to aid in comparing these results with those in the previous section, we maintain $\delta_t = 0.025$.

Using the same methodology and range of values in parameter space (C_t, C_l), Fig. 4b shows the results of numerical integration of Eq. 3. These results are to be compared to those in Sect. 1.

- Numerous boundaries exist between SASSM, DASSM, and TASSM in parameter space (C_t, C_l) when the microcantilever damping δ_l is decreased. This is due to the lower dissipation rate which increases the probability of DASSM and TASSM relative to the probability of a SASSM.
- Since δ_t remains unchanged, for large C_t and low C_l Fig. 4a is very similar to Fig. 4b. This similarity is due to the fact that δ_t and C_l dominate the response for large C_t .
- Due to the lower dissipation in microcantilever, a ‘random’ point selected in Fig. 4b has a greater probability of being a DASSM or TASSM. This may be understood using Fig. 5. Since the damping is decreased, in Fig. 5c, for example, the probability of the tip moving past B_2^- to rest in B_3 is much greater than in the higher dissipation case presented in Fig. 4a.
- Numerous transitional boundaries between SASSM, DASSM, and TASSM are present for this lower tip dissipation case. The reason for the increased number of boundaries is evident when phase space is examined. Each progressive boundary corresponds to an additional rotation in the manifold boundary separating SASSM from DASSM. The coiling of the manifold boundaries in phase space for low C_t results in the striped pattern shown in Fig. 4b.
- Figure 4a and b both suggest that as the cantilever compliance is increased, while keeping the tip

compliance constant, then the number of slips changes in a non-monotonic manner. This can be explained as follows. When the cantilever compliance is small, its deflection just prior to a slip event is very small, possibly less than an atom spacing. Consequently, the tip slips very little. As the cantilever compliance increases, its deflection prior to a slip event is large, of the order of multiple atom spacings. Then following the sudden release during a slip event, the transient oscillations can span several atoms. However, the precise atom to which the tip sticks to following the slip event is dictated by the domain of attraction of each atom. Thus for highly compliant cantilevers, while the probability of multiple atom slips increases, the actual number of atoms passed is closely connected to the domains of attraction of the transient cantilever and tip dynamics, and can change non-monotonically.

In summary, the main effect of changing microcantilever damping is to modify the rate of energy dissipation. By decreasing the rate of energy dissipation, a larger number of atoms are involved in the sudden slip event.

In Fig. 4c, the parameter values for which prior experiments have been performed are compared to the non-dimensional parameters in the present work. The work of Medyanik et al. [3] observes DASSM experimentally by increasing the normal load, however, since they use conventional microcantilevers, their tip compliances are low. In the work of Ishikawa et al. [12], the normal load is not increased to a high enough value to observe DASSM. And the work of Socoliuc et al. [4] focuses on the regime of steady sliding for very low normal loads, corresponding to both very low tip and cantilever compliance.

5 Force Calculations

We now turn our attention to the magnitude of the average lateral forces encountered during a SASSM, DASSM, or TASSM. For slow sliding speeds, the quasi-static model provides an accurate understanding of the forces involved in moving the microcantilever at constant velocity. The average measured frictional force, $\langle F_{\text{meas}} \rangle$, is simply the mean value of the measured lateral force averaged over a complete period of length T :

$$\langle F_{\text{meas}} \rangle = \frac{1}{T} \int_{Y=0}^T C_e F_{\text{meas}} dY. \quad (10)$$

This integration is performed for varying C_e , and a specified SASSM ($T = 1$), DASSM ($T = 2$), or TASSM ($T = 3$). The integrand is simply a scaled version of the results presented in Fig. 3 which is integrated numerically in Matlab. The results of this numerical integration are

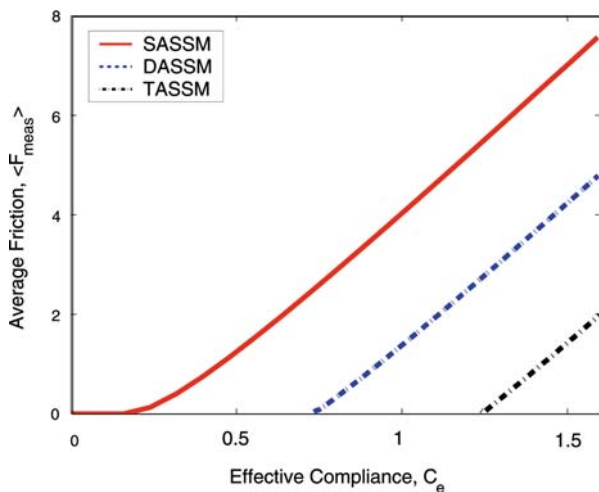


Fig. 6 Average frictional force $\langle F_{\text{meas}} \rangle$ based on static considerations as a function of effective compliance, C_e . For the same effective compliance, C_e , the average frictional forces, $\langle F_{\text{meas}} \rangle$ is reduced for multiple atom stick-slips when compared to SASSMs

presented in Fig. 6. Several observations can be made from Fig. 6:

- For $C_e < C_e^{(1)}$, $\langle F \rangle = 0$. This implies that if the microcantilever steadily slides over the surface, there will be no average frictional force. This corresponds to the regime of superlubricity discussed recently [4]. However, once $C_e > C_e^{(1)}$, the average frictional force increases steadily.
- The results of the average friction force for DASSM and TASSM have not previously been reported.
- The average lateral forces during a TASSM are lower than for a DASSM, which in turn are lower than for a SASSM. This implies that if a stick-slip motion occurs, maximizing the number of atoms, the tip suddenly slips over will decrease the average friction force. In this sense, the work presented in this article indicates that the lateral friction forces can be modified by tailoring the C_e values.

6 Conclusions

The influence of tip compliance on the onset of single and multiple atom stick-slip motions has been investigated by adapting Tomlinson's model to account for tip compliance. The key findings of the work are:

1. Static considerations lead to analytical expressions for effective compliance that separate steady sliding motions from the possibility of single or multiple atom stick-slip events.

2. To predict whether a single or multiple atom stick-slip event will actually occur requires an investigation of the nonlinear dynamics of the tip following a slip event.
3. Depending on the level of microcantilever damping, multiple boundaries appear in parameter space that separate regimes corresponding to single or multiple stick-slip events.
4. The relative compliances of the tip and microcantilever determine whether a specific atom stick-slip event is likely to occur or not. Since the lateral force depends on the number of atoms bypassed in a stick-slip event, the relative compliances in effect also control the magnitude of lateral friction forces. The impact of tip compliance may aid in understanding the results of Medyanik et al. [3]. In most experimental cases, a lower normal load was required than predicted experimentally. Including the effects of tip compliance may improve the theoretical model.
5. By varying the tip and microcantilever compliances, it is possible to have transition from a SASSM to a DASSM, and thus decrease the mean friction force experienced by the tip.
6. Finally, the results also have certain implications for experimental friction force microscopy. For instance, the relative compliances could place the system near a boundary in parameter space that separates say a single from a double atom stick-slip motion. Under small perturbations, the tip could then evolve either to a single or double atom stick-slip motion, even while the sample surface is homogeneous. In other words, this would lead to artificial friction force variations even on a homogeneous sample.

The present work has focused on examining the effects of tip and cantilever compliance in the slowest possible speed limit. Interesting future work could include a study of the velocity dependence of the multiple atom stick-slip motions.

Acknowledgments The primary author (WGC) would like to acknowledge the support of the Department of Energy via a Computational Science Graduate Fellowship (CSGF) administered by the Krell Institute. The corresponding author (AR) would like to acknowledge the support of the National Science Foundation through Grant 0409660-CMS.

References

1. Mate, C.M., McClelland, G.M., Erlandsson, R., Chiang, S.: Atomic-scale friction of a tungsten tip on a graphite surface. *Phys. Rev. Lett.* **59**, 1942–1945 (1987)
2. Meyer, E., Overney, R.M., Dransfeld, K., Gyalog, T.: *Nanoscience: Friction and Rheology on the Nanometer Scale*. World Scientific, Singapore (1998)

3. Medyanik, S.N., Liu, W.K., Sung, I.-H., Carpick, R.W.: Predictions and observations of multiple slip modes in atomic-scale friction. *Phys. Rev. Lett.* **97**, 136106 (2006)
4. Socoliuc, A., Bennewitz, R., Gnecco, E., Meyer, E.: Transition from stick-slip to continuous sliding in atomic friction: entering a new regime of ultralow friction. *Phys. Rev. Lett.* **92**, 134301 (2004)
5. Braiman, Y., Barhen, J., Protopopescu, V.: Control of friction at the nanoscale. *Phys. Rev. Lett.* **90**, 094301 (2003)
6. Cochard, A., Bureau, L., Baumberger, T.: Stabilization of frictional sliding by normal load modulation. *Trans. ASME* **70**, 220–226 (2003)
7. Rozman, M.G., Urbakh, M., Klafter, J.: Controlling chaotic frictional forces. *Phys. Rev. E* **57**, 7340–7343 (1998)
8. Conley, W.G., Raman, A., Kroussgrill, C.M.: Nonlinear dynamics in Tomlinson's model for atomic scale friction and friction force microscopy. *J. Appl. Phys.* **98**, 053519 (2005)
9. Persson, B.N.J.: *Sliding Friction Physical Principles and Applications*. Springer, New York (2000)
10. Porto, M., Zaloj, V., Urbakh, M., Klafter, J.: Macroscale vs. microscale description of friction: from Tomlinson to shearons. *Tribol. Lett.* **9**, 45–54 (2000)
11. Tomlinson, G.A.: A molecular theory of friction. *Phil. Mag.* **7**, 905–939 (1929)
12. Ishikawa, M., Yoshimura, M., Ueda, K.: Carbon nanotube as a probe for friction force microscopy. *Physica B* **323**, 184–186 (2002)
13. Luan, B., Robbins, M.O.: Effect of inertia and elasticity on stick-slip motion. *Phys. Rev. Lett.* **93**, 036105-1 (2004)
14. Johnson, K.L., Woodhouse, J.: Stick-slip motion in the atomic force microscope. *Tribol. Lett.* **5**, 155–160 (1998)
15. Hölscher, H., Schwarz, U.: Modelling of the scan process in lateral force microscopy. *Surf. Sci.* **375**, 395–402 (1997)
16. Carpick, R.W., Ogletree, D.F., Salmeron, M.: Lateral stiffness: a new nanomechanical measurement with friction force microscopy. *Appl. Phys. Lett.* **70**, 1548–1550 (1997)
17. Lantz, M.A., O'Shea, S.J., Hoole, A.C.F., Welland, M.E.: Lateral stiffness of the tip and tip-sample contact in frictional force microscopy. *Appl. Phys. Lett.* **70**, 970–972 (1997)
18. Wiggins, S.: *Introduction to Applied Nonlinear Dynamical Systems and Chaos*. Springer-Verlag, New York (1990)
19. Sharos, L.B., Raman, A., Crittenden, S., Reifenberger, R.: Enhanced mass sensing using torsional and lateral resonance in microcantilevers. *Appl. Phys. Lett.* **84**, 4638–4640 (2004)